$^{16}O(e, e'\alpha)^{12}C$ measurements and the $^{12}C(\alpha, \gamma)^{16}O$ astrophysical reaction rate

D. H. Potterveld,[1,*] B. W. Filippone,[2,†] R. J. Holt,[2,‡] and I. Friščić[3,§]

[1]*Physics Division, Argonne National Laboratory, Argonne, Illinois 60439, USA*

[2]*Kellogg Radiation Laboratory, California Institute of Technology, Pasadena, California 91125, USA*

[3]*Department of Physics, Faculty of Science, University of Zagreb, Bijenička c. 32, 10000 Zagreb, Croatia*

(Received 20 December 2023; revised 7 June 2024; accepted 8 August 2024; published 19 September 2024)

The $^{12}C(\alpha, \gamma)^{16}O$ reaction, an important component of stellar helium burning, has a key role in nuclear astrophysics. It has significant impact on the evolution and final state of heavy to low mass stars, maximum mass of stellar formed black holes and also shapes the elemental abundances resulting from nucleosynthesis in such stars. Providing a reliable estimate for the energy dependence of this reaction at stellar helium burning temperatures has been a longstanding and important goal. In this work, we study the role of potential new $E1$ and $E2$ measurements of the $^{16}O(e, e'\alpha)^{12}C$ reaction in reducing the overall uncertainty in the astrophysical S factor for the $^{12}C(\alpha, \gamma)^{16}O$ $E1$ and $E2$ ground state capture extrapolated to a stellar energy of 300 keV. A multilevel R-matrix analysis is used to make extrapolations of the $S_{E1}(300\ \text{keV})$ and $S_{E2}(300\ \text{keV})$ factors for the $^{12}C(\alpha, \gamma)^{16}O$ reaction from existing ground state capture data. Bayesian analysis is used to quantify the uncertainties in the extrapolations for both the existing data alone and also when possible new experimental data are included. In particular, we consider a new experiment that would make use of a high-intensity low-energy electron beam that impinges on a windowless oxygen gas target as a means to determine the total $E1$ and $E2$ ground state cross sections for this reaction. We find that the new data could significantly reduce the $S(300)$ uncertainties. Splitting the new data into high and low energy regions shows that both low and high energy data are effective in reducing the uncertainty.

DOI: 10.1103/PhysRevC.110.035809

I. INTRODUCTION

The $^{12}C(\alpha, \gamma)^{16}O$ (CTAG) cross section is essential in nuclear astrophysics [1,2]. Recent reviews illustrate the importance of this reaction in both the evolution of and nucleo-synthetic yields from massive stars [3] as well as low to intermediate mass stars [4]. Recent work [5,6] has noted the importance of this reaction in determining the maximum mass of stellar-formed black holes. The purpose of this study is to explore the role that future measurements of the $^{16}O(e, e'\alpha)^{12}C$ (OSEEA) reaction could have on reducing the overall uncertainty in the cross section for the $^{12}C(\alpha, \gamma)^{16}O$ reaction at helium burning temperatures. To do this, we first perform a Bayesian evaluation of uncertainty for existing CTAG data, and then perform a second round of Bayesian updating to include possible new data from a proposed OSEEA experiment. In particular, we consider a proposed experiment [7] in which the $E1$ and $E2$ $^{12}C(\alpha, \gamma)^{16}O$ ground state cross sections can be extracted [7], and for which the authors have predicted statistical uncertainties. However, the framework we have used can also easily accommodate data from other possible experiments, such as inverse reaction $^{16}O(\gamma, \alpha)^{12}C$ (OSGA) experiments [8–12] enabled by proposed high intensity photon sources [13–15].

Stellar helium burning usually occurs at a low energy, conventionally discussed at a representative Gamow peak energy of 300 keV. As is well known, the CTAG cross section at this energy is extremely small, to date precluding direct measurement in the laboratory. The usual approach to this problem has been to extend cross section measurements to as low an energy as possible, and then extrapolate a fitted R-matrix theory model to 300 keV. An excellent review of this subject, with a detailed R-matrix analysis of the CTAG reaction is given in Ref. [3]. The existing world CTAG data represent many decades of effort to measure cross sections at the lowest practical energy.

One of the complicating issues for the R-matrix extrapolation is that resonances associated with higher energy states in the ^{16}O compound nucleus have significant effect at much lower energies, and vice versa, because of interference effects. Thus, the R-matrix model needs to include states well above threshold for accurate calculation of low energy cross sections. We will show that, similarly, cross section measurements at energies well above the Gamow energy can provide significant constraint on the low energy extrapolation. Therefore, in our work, we have considered data, existing and proposed, up to 6.35 MeV in the center of mass. We employed the R-matrix approach to calculate the total $E1$ and $E2$ cross sections, $\sigma(E)$, for CTAG to the ground state. We considered only ground state capture for this study since the capture to

*Contact author: potterveld@anl.gov

†Contact author: bradf@caltech.edu

‡Contact author: rholt@caltech.edu

§Contact author: ifriscic.phy@pmf.hr

excited states is believed [3] to contribute only about 5% to the total capture rate at 300 keV. The cross section is then used to calculate the astrophysical S factor given by

$$S(E) = \sigma(E)Ee^{2\pi\eta}, \tag{1}$$

where E is the energy in the center of mass, η is the Sommerfeld parameter, $\sqrt{\frac{\mu}{2E}}Z_1Z_2\frac{e^2}{\hbar}$, and μ is the reduced mass of the carbon ion and α particle.

The approach we have taken to assess the impact of potential new experimental data is to perform a sequence of Bayesian uncertainty analyses. We adopt 'maximum *a posteriori* probability' (MAP) as the estimator for parameter values, and the square root of the variance from this estimate (using the posterior distribution for weighting) as the estimator of uncertainty. To proceed, we first construct an R-matrix model based on physical parameters: resonance energies and their widths with values and uncertainties taken from the literature. This model is fit to the existing CTAG world data for $E1$ and $E2$, and the first round of Bayesian analysis produces uncertainty estimates for the model parameters and $S(300)$. In this round, the literature values are the 'priors', and the CTAG data are the new evidence. We then evaluate the fitted model at possible OSEEA experiment energies to construct an unbiased set of hypothetical new measurements. Statistical uncertainties for these new data are computed from a Monte Carlo simulation of the OSEEA experiment. Finally, an second round of Bayesian updating is performed to obtain new uncertainties for the parameters and astrophysical S factors. The change in uncertainties is the prediction of the impact of the new data.

II. CTAG *R*-MATRIX MODEL

We employ the R-matrix code AZURE2 [16] in the present work. In the R-matrix formalism, the $E1$ and $E2$ multipolarities proceed through states of different J^π, so that the $E1$ and $E2$ cross sections are nearly independent, having only the ground state asymptotic normalization coefficients (ANCs) as parameters in common. We therefore treat $E1$ and $E2$ data separately, to reduce the number of parameters to be fit at one time.

Unlike previous studies [17–19], we include the external part [20] of the R-matrix and higher energy capture data for this study. Since the external part of the R-matrix analysis is far more sensitive to the $E2$ cross section than the $E1$ cross section, we begin with fits to the $E2$ data in order to constrain the ^{16}O ground state asymptotic normalization coefficient, ANC(0^+), which governs the external part. The $E1$ analysis that follows uses the updated ANC(0^+) value and uncertainty, and therefore the $E2$ and $E1$ analyses are actually two sequential rounds of Bayesian updating themselves.

As before, we only consider ground state transitions and statistical errors in this study. We chose a channel radius of 5.43 fm for the α channel to be consistent with a previous analysis [3]. We also include in the analysis the ^{15}N$(p,\gamma)^{16}$O channel (with radius 5.03 fm), because it was found to have a significant effect on the CTAG $E1$ cross sections at center of mass energies above 5.5 MeV.

TABLE I. R-matrix model parameters and analysis results for the CTAG $E2$ channel with a channel radius of 5.43 fm. The widths for resonances above threshold are the observable widths $\Gamma_{\lambda\alpha}$. The ground state ANC for the α channel is labeled ANC(0^+) and the $E2\,\alpha$ bound state is represented by ANC(2^+). The bound proton channel ANC's are labeled and the unbound proton channel width is labeled $\Gamma_{\lambda p}$. The minus signs in front of the widths indicate the signs of the corresponding reduced width amplitudes. The literature values for the parameters are those tabulated in Ref. [3] or, where they exist, the new values calculated in that work (using the larger of the calculated statistical or systematic uncertainty) with the following exceptions: The literature values for ANC(0^+) and ANC(2^+) were taken from the weighted averages and uncertainties in Table II and illustrated in Fig 1, E_5 is taken from Ref. [21], and several unknown and irrelevant resonance widths were fixed to zero. Parameters for which no prior literature value exists are indicated by 'n/a'. Also tabulated are our fitted values and uncertainties, as discussed in the text.

Parameter	Literature value	Fixed value	Fitted value	Units
ANC(0^+)	417(80)		367(51)	$\mathrm{fm}^{-1/2}$
ANC$p(0^+)$	13.9(19)		13.9(19)	$\mathrm{fm}^{-1/2}$
E_1	6.9171(6)		6.9170(6)	MeV
ANC(2^+)	1.264(78)		1.331(66)	$10^5\ \mathrm{fm}^{-1/2}$
$\Gamma_{1\gamma}$	97(3)		97.6(30)	meV
ANCp_1	0.45(13)		0.45(13)	$\mathrm{fm}^{-1/2}$
E_2	9.8445(5)		9.8445(5)	MeV
$\Gamma_{2\alpha}$	0.62(10)		0.60(10)	keV
$\Gamma_{2\gamma}$	−5.7(6)		−5.6(6)	meV
ANCp_2	n/a	0		$\mathrm{fm}^{-1/2}$
E_3	11.5055(5)		11.5055(5)	MeV
$\Gamma_{3\alpha}$	83.0(60)[a]		81.0(22)	keV
$\Gamma_{3\gamma}$	−0.49(10)[a]		−0.75(5)	eV
ANCp_3	n/a	0		$\mathrm{fm}^{-1/2}$
E_4	12.9656(28)		12.9656(28)	MeV
$\Gamma_{4\alpha}$	−349.0(80)		−349.0(80)	keV
$\Gamma_{4\gamma}$	−0.56(19)[a]		−0.61(15)	eV
Γ_{4p}	1.82(20)		1.82(20)	keV
E_5	14.926(2)	14.926		MeV
$\Gamma_{5\alpha}$	n/a		13.1(11)	MeV
$\Gamma_{5\gamma}$	n/a	0		eV
Γ_{5p}	n/a	0		keV

[a]Omitted from the Bayesian 'prior' as discussed in the text.

For $E2$, we use the five lowest known 2^+ resonance levels in the R-matrix model, which therefore has 22 parameters, shown in Table I. The fifth level is positioned at the known energy of 14.926 MeV, but the α width is used as a background pole term that represents the combined effect of higher energy resonances.

For ANC(0^+), and to lesser extent ANC(2^+), there is significant dispersion among published values, as shown in Table II and illustrated in Fig. 1. We use the weighted averages for the literature values, with uncertainties scaled by the Birge factor [22] to make χ^2 per degree of freedom equal to 1.

None of the proton parameters have a significant effect on the $E2$ cross section at energies of the existing data, and therefore they are not relevant to the astrophysical S factor.

TABLE II. Values of ANC(0^+) and ANC(2^+) from α-^{12}C elastic scattering and transfer reactions from Refs. [23–33] used in the present fits. The uncertainties on the weighted averages are determined by multiplying the weighted errors by the Birge factors [22].

ANC data	ANC(0^+) ($\text{fm}^{-\frac{1}{2}}$)	ANC(2^+) ($10^5\ \text{fm}^{-\frac{1}{2}}$)
Brune (1999)	–	1.14 (10)
Buchmann (2001)	–	2.28 $(^{+33}_{-37})$
Belhout (2007)	–	1.40 $(^{+50}_{-45})$
Matei (2008)	–	2.3 (4)
Tischhauser (2009)	–	1.54 (18)
Oulebsir (2012)	–	1.44 (28)
Avila (2015)	–	1.22 (7)
Adhikari (2017)	637 (86)	1.67 (23)
Shen (2019)	–	1.05 (14)
Shen (2020)	337 (45)	1.55 (9)
Mondal (2021)	471 (75)	1.03 (8)
weighted avg	417 (80)	1.264 (78)

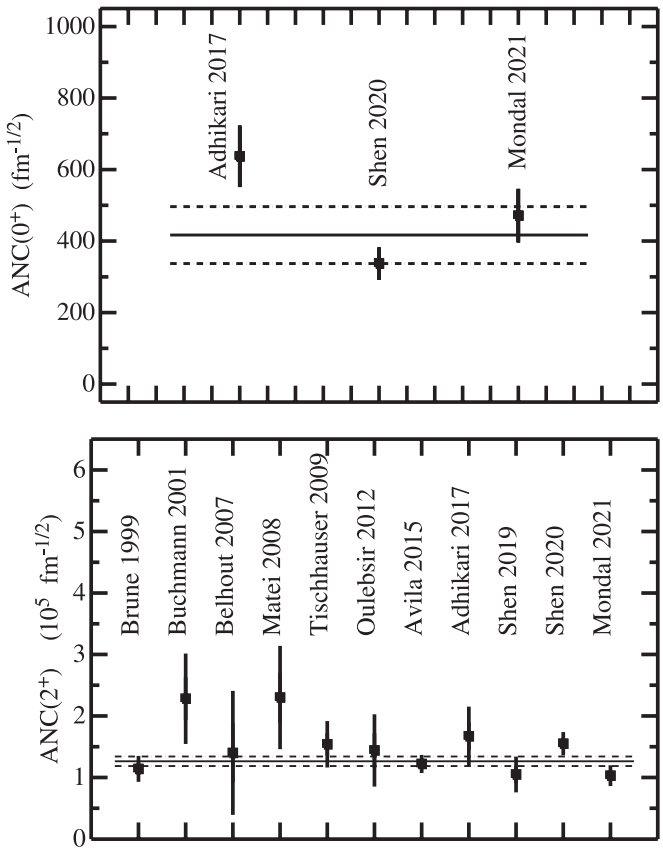

FIG. 1. Comparison of previous ANC(0^+) and ANC(2^+) results. The weighted averages were used as the literature values in the present fits. The previous ANC results were taken from Refs. [23–33]. The error limits represent the weighted errors multiplied by the Birge factors [22].

However, where literature values for these parameters are known, we allow the parameters to vary in our analysis. They are constrained by the literature data, and this provides a cross-check on our analysis method, which must recover the literature value and uncertainty. Similarly, the parameter $\Gamma_{5\gamma}$ is found not to significantly affect the $E2$ cross section at existing data energies, and is set to zero. The literature values for the parameters $\Gamma_{3\alpha}$, $\Gamma_{3\gamma}$, and $\Gamma_{4\gamma}$ come from Ref. [3], which used the existing CTAG data in its analysis. We allow these parameters to vary in our analysis, but omitted the literature values from the computation of the Bayesian 'prior' discussed in the following section, because the data will be used in the Bayesian 'evidence' instead.

The R-matrix model for $E1$ is composed in the same way as $E2$, using the five lowest known 1^- resonances, with the energy of the highest resonance fixed at its literature value, and the α width of this resonance serving as a background pole term. One difference is that we use our results for ANC(0^+) from the $E2$ analysis as the 'literature' value entering into the computation of the 'prior'. This makes our $E1$ analysis a second round of Bayesian updating. A second difference is that we allow the gamma width of the highest resonance to vary, as it has a strong influence on the χ^2 of the fit. As with $E2$, we set unknown and irrelevant proton parameters to zero, and we suppress three parameters when computing the Bayesian 'prior', because existing CTAG data were used in producing those literature results. The literature values and results of our analysis for $E1$ (discussed in the following section) are shown in Table III.

III. SYSTEMATIC UNCERTAINTY IN THE NORMALIZATION OF MEASURED CROSS SECTIONS

As pointed out in [3], experimentally measured cross sections are subject to systematic uncertainty in the overall normalization of the results. In a global analysis of several independently normalized experiments, the normalizations tend to average out in the fitting of a model to all the data, but their uncertainty can potentially increase the uncertainty of the fitted parameters. These normalizations were explicitly included in our analysis as auxiliary model parameters that scale the measured cross sections and uncertainties by a constant factor, using separate factors for each independent data set. These normalization factors have an *a priori* expected value of 1.0, and uncertainty as reported in the literature. We included these normalization parameters in our fitting and uncertainty analysis, on equal footing with the R-matrix model parameters, assuming a Gaussian probability distribution for each independent normalization. Where no uncertainty was reported for an experiment, we have assumed a 10% uncertainty. The normalization factors, uncertainties, fitted values, and their uncertainties from our Bayesian analysis are shown in Table IV.

We also performed a simpler analysis in which all the normalizations were fixed at 1. All of the fitted parameters in that analysis differed from the rigorous analysis by less than the uncertainties in Tables I and III. Most of the uncertainties were also in agreement, however the uncertainties in the $E1$ parameters $\Gamma_{2\gamma}$, $\Gamma_{3\gamma}$, and $\Gamma_{4\gamma}$ were significantly underestimated.

TABLE III. *R*-matrix model parameters and analysis results for the CTAG $E1$ channel, using the naming and sign conventions of Table I. The literature values are those tabulated in Ref. [3] or, where they exist, the new values calculated in that work (using the larger of the calculated statistical or systematic uncertainty), with the following exceptions: ANC(0^+) and ANCp(0^+) are from our fit for $E2$ data. Parameters for which no prior literature value exists are indicated by 'n/a'. E_1, E_4, and E_5 are from Ref. [21].

Parameter	Literature value	Fixed value	Fitted value	Units
ANC(0^+)	367(51)		367(50)	$\mathrm{fm}^{-1/2}$
ANCp(0^+)	13.9(19)		13.9(19)	$\mathrm{fm}^{-1/2}$
E_1	7.11685(14)		7.11687(13)	MeV
ANC(1^-)	2.08(20)		2.04(17)	$10^{14}\ \mathrm{fm}^{-1/2}$
$\Gamma_{1\gamma}$	55(3)		54.9(30)	meV
ANCp_1	0.98(12)		0.98(12)	$\mathrm{fm}^{-1/2}$
E_2	9.586(8)		9.577(3)	MeV
$\Gamma_{2\alpha}$	382(4)		385.9(35)	keV
$\Gamma_{2\gamma}$	−15.6(12)[a]		−14.55(36)	meV
ANCp_2	n/a	0		$\mathrm{fm}^{-1/2}$
E_3	12.4493(8)		12.4497(8)	MeV
$\Gamma_{3\alpha}$	99.2(11)		99.9(10)	keV
$\Gamma_{3\gamma}$	5.6(9)[a]		7.36(75)	eV
Γ_{3p}	1.73(20)		1.60(20)	keV
E_4	13.090(8)		13.083(2)	MeV
$\Gamma_{4\alpha}$	−29.9(6)		−30.31(60)	keV
$\Gamma_{4\gamma}$	42(8)[a]		55.1(57)	eV
Γ_{4p}	110.4(5)		110.7(5)	keV
E_5	16.20(9)	16.20		MeV
$\Gamma_{5\alpha}$	n/a		8.55(50)	MeV
$\Gamma_{5\gamma}$	n/a		−0.57(18)	eV
Γ_{5p}	n/a	0		keV

[a]Omitted from the Bayesian 'prior' as discussed in the text.

TABLE IV. Difference from unity for the normalization factors and their uncertainties. The tabulated values are $1000(f-1)$, where f is the normalization factor. Uncertainties have the same scale. The data sets are Refs. [34–45].

	$E1$ normalization		$E2$ normalization	
Data set	*a priori*	fitted	*a priori*	fitted
Assuncao	0(20)	8(18)	0(20)	−2(20)
Brochard[a]	0(100)	5(100)		
Dyer	0(100)	−6(29)		
Gialanella	0(100)	−150(31)		
Kremer	0(150)	75(60)		
Kunz[b]	0(100)	−13(45)	0(100)	−85(68)
Makii[a]	0(100)	32(61)	0(100)	−10(89)
Ouellet[b]	0(60)	−52(25)	0(60)	−11(51)
Plag	0(120)	46(93)	0(300)	−40(200)
Redder[b]	0(60)	−52(25)		
Roters[a]	0(100)	17(38)	0(100)	15(87)
Schurmann	0(65)	−2(65)	0(65)	41(55)

[a]No published value for systematic uncertainty; 10% assumed.
[b]These experiments reference the same cross section for normalization.

This confirms the importance of a rigorous treatment of normalization uncertainties.

IV. CTAG FITTING AND BAYESIAN UNCERTAINTY ANALYSIS

Both the fitting of model parameters (*R*-matrix parameters and the auxiliary normalization factors) and the determination of parameter uncertainties involve the construction of a 'posterior' probability distribution from conditional probabilities through Bayes's theorem [46]:

$$P(H|E) = \frac{P(H)\cdot P(E|H)}{P(E)}, \tag{2}$$

in which $P(H|E)$ is the probability of hypothesis H given new evidence E, $P(H)$ is the probability of the hypothesis before the new evidence is introduced, $P(E|H)$ is the likelihood or agreement of the evidence with the hypothesis, and $P(E)$ is the probability of the evidence. $P(H)$ and $P(H|E)$ are conventionally called the 'prior' and 'posterior' probabilities. $P(E)$ is the integral of the numerator on the right hand side of Eq. (2) over all possible hypotheses (or sum in the case of discreet hypotheses) and may be absorbed into the normalization of $P(H|E)$.

In our work, any specific set of values for the model parameters constitutes a hypothesis H, and CTAG cross section measurements are the evidence E. We assume Gaussian-distributed statistical uncertainties for the data, and calculate $P(E|H)$ from the χ^2 of the data relative to the model

$$\ln P(E|H) = -\tfrac{1}{2}\chi^2_{\mathrm{data}} + \mathrm{const}, \tag{3}$$

in which

$$\chi^2_{\mathrm{data}} = \sum\left(\frac{Y_i - Y_i^H}{\Delta Y_i}\right)^2, \tag{4}$$

where the Y_i are the experiment data, ΔY_i are their uncertainties, and Y_i^H are the model values.

The Bayesian 'prior', the probability of a specific set of parameter values, is defined as

$$\ln P(H) = -\tfrac{1}{2}\chi^2_{\mathrm{param}} + \mathrm{const}, \tag{5}$$

in which

$$\chi^2_{\mathrm{param}} = \sum\left(\frac{X_i - X_i^{\mathrm{lit}}}{\sigma_i}\right)^2, \tag{6}$$

where the X_i are the model parameters, X_i^{lit} are the literature values (for *R*-matrix parameters) or 1.0 (for data set normalizations), σ_i are the corresponding uncertainties, and we have assumed independent, Gaussian probability distributions for each parameter. The sum does not include *R*-matrix model parameters for which literature values were determined using CTAG data, because CTAG data should enter the posterior through the evidence, and not the prior.

Applying Bayes's theorem yields

$$\begin{aligned}\ln P(H|E) &= \ln P(H) + \ln P(E|H) + \mathrm{const.}\\ \ln P(H|E) &= -\tfrac{1}{2}\left(\chi^2_{\mathrm{param}} + \chi^2_{\mathrm{data}}\right) + \mathrm{const.}\end{aligned} \tag{7}$$

The MAP estimate of the parameter values for the combination of the prior (literature values) plus new evidence (world CTAG data) is obtained by finding the parameter combination that minimizes $\chi^2_{\rm tot}$:

$$\chi^2_{\rm tot} = \chi^2_{\rm param} + \chi^2_{\rm data}. \tag{8}$$

The parameters X_i are continuous variables, so that the posterior $P(H|E)$ (hereafter just P) is a continuous probability density function. For a quantity $Z(X_i)$, we define the uncertainty ΔZ to be the square root of the P-weighted variance:

$$(\Delta Z)^2 = \int (Z - Z_0)^2 \cdot P\, dX_1 \ldots dX_n, \tag{9}$$

where Z_0 is the value of Z for the 'best' X_i, i.e., the ones that minimize $\chi^2_{\rm tot}$. This is, of course, the definition of standard error for a normally distributed Z, and one might prefer an alternative (e.g., full width half-maximum) for skewed or heavy-tailed distributions for which the variance is infinite. But it turns out, for the data analyzed here, P is very well approximated by a multivariate normal distribution (MVND), and the astrophysical S factors at the Gamow energy are dominantly linear in the R-matrix parameters, so that using standard errors makes sense.

To minimize $\chi^2_{\rm tot}$ with respect to the model parameters X_i, we use the method of Hooke-Jeeves, as implemented in the NIMROD/O software package [47]. NIMROD/O is a framework for parallelized multivariate function minimization using an external program (in this case AZURE2) to perform function evaluations. We first attempted to use more conventional gradient-based nonlinear minimization algorithms, but these often failed to converge because of noise in the AZURE2 results that affects the numerical computation of derivatives.

Hooke-Jeeves is a derivative-less pattern search algorithm that uses an adaptive step size, and this was found to robustly converge to the correct minima. The noise in the AZURE2 output was investigated and found to arise in the conversion of physical parameters to formal R-matrix parameters. It only occurs with variation of the energy parameter E_1 in both the $E2$ and $E1$ calculations; the results are smooth for variation of the other parameters. The effect of the noise is illustrated in Fig. 2, in which E_1 in the $E2$ model is varied in steps of 0.5 eV about the fitted value of 6916921 eV, with all other parameters held at their fitted values. The $\chi^2_{\rm tot}$ is randomly dispersed in a band of thickness ≈0.05 near the origin. The $E1$ model shows similar behavior. Although this interferes with numerical differentiation, the uncertainty in determining the location of the minimum via Hooke-Jeeves is ≈50 eV, which is much smaller than the 600 eV uncertainty of the literature value. Therefore, this noise does not contribute significantly to our results, and we have ignored it.

The fit for $E2$ results in a $\chi^2_{\rm tot}$ of 51.3, for 68 data points, 24 fitted parameters, and 20 literature values contributing to the 'prior'. There are therefore 64 degrees of freedom, and the fit has a P value of 0.87. The S factor for the fitted model is plotted together with the CTAG data in Fig. 3. Extrapolating the fitted model to the Gamow energy yields an astrophysical S factor $S_{E2}(300) = 48.9$ keV b.

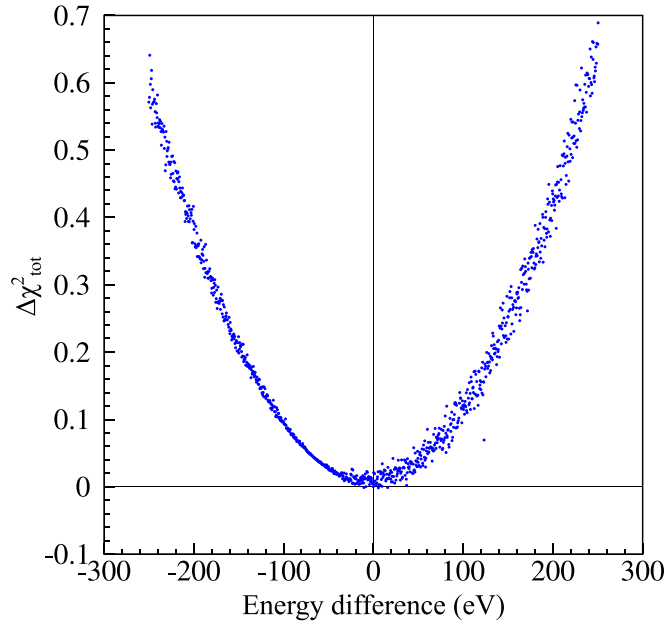

FIG. 2. The change in $\chi^2_{\rm tot}$ from the best fit for the $E2$ data is plotted as the parameter E_1 is varied in steps of 0.5 eV, with all other parameters fixed at their fitted values. The best fit found via the Hooke-Jeeves method is the origin of the graph.

The $E1$ fit has 187 data points, 30 fitted parameters, and 25 literature values contributing to the 'prior', for 182 degrees of freedom. Fitting the data with the quoted uncertainties resulted in a minimum $\chi^2_{\rm tot}$ much larger than this. We chose to address this by multiplying the statistical uncertainty of each data point by a constant factor of 1.26. This decreases $\chi^2_{\rm data}$ by a factor of $1/(1.26)^2$, while not affecting $\chi^2_{\rm param}$. This drives the fit slightly toward the literature values, and increases the uncertainty in fitted parameter values and S factors. This is

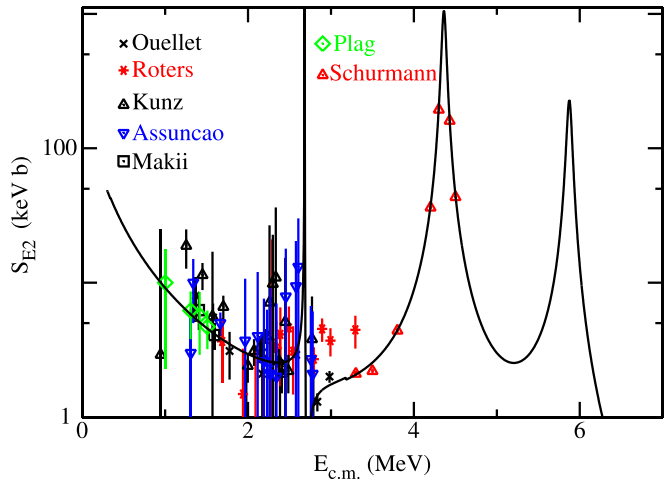

FIG. 3. The astrophysical S factors for the $E2$ cross section as a function of center of mass energy. The solid black line represents the fit curve with parameters from Table I. The existing $E2$ data were taken from Refs. [34–40].

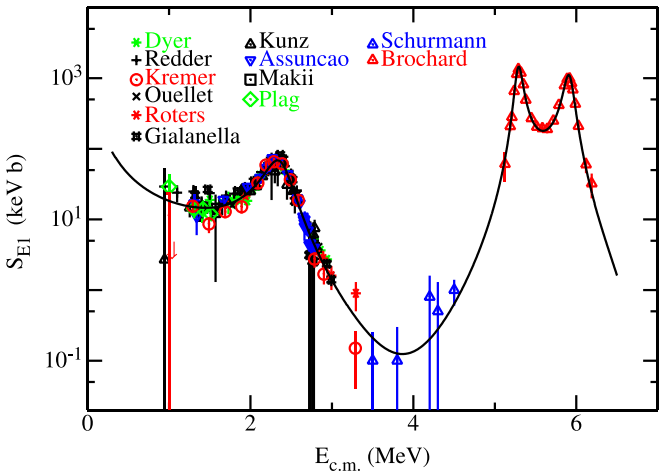

FIG. 4. The astrophysical S factors for the $E1$ cross section as a function of center of mass energy. The solid black line represents the fit curve with parameters from Table III. The existing data were taken from Refs. [34–45].

a conservative and minimally biased way to account for the nonstatistical scatter in the CTAG data.

The fit with rescaled uncertainties results in a $\chi^2_{\rm tot}$ of 172.9, and a P value of 0.67. The S factor for the fitted model is plotted together with the CTAG data in Fig. 4. Extrapolating the fitted model to the Gamow energy yields an astrophysical S factor $S_{E1}(300) = 91.4$ keV b.

Uncertainties in the model parameters and the astrophysical S factors are calculated by numerically integrating Eq. (9). This is an indefinite integral over a high dimension space with a computationally expensive integrand. We employ an 'importance sampling' technique that we have not seen applied before to Bayesian uncertainty quantification, and which has significant advantages to the ubiquitous technique of Markov chain Monte Carlo (MCMC).

We begin by rewriting Eq. (9) as

$$(\Delta Z)^2 = \int (Z - Z_0)^2 \cdot \left(\frac{P}{Q}\right) d^n[C], \tag{10}$$

where

$$Q(X_1, \ldots, X_n) = \frac{d^n[C]}{dX_1 \ldots dX_n} \tag{11}$$

and C is as yet unspecified. One special case is to define $Q = P$, so that C is the cumulative distribution function (CDF) for P. This would result in

$$(\Delta Z)^2 = \int (Z - Z_0)^2 \, d^n[C], \tag{12}$$

which can be numerically integrated by uniformly sampling C. This is what MCMC does.

Our approach is to let Q be a MVND, defined as

$$\ln Q = -\frac{1}{2} \sum_{i,j} [\mathrm{cov}]^{-1}_{ij} X_i X_j + \mathrm{const}, \tag{13}$$

where [cov] is the covariance matrix. It is easy to generate uncorrelated, pseudorandom vectors X_i that uniformly sample the CDF of a MVND so that

$$(\Delta Z)^2 = < W \cdot (Z - Z_0)^2 >, \tag{14}$$

in which we compute a weighted average over the random samples with weight $W = P/Q$. This approach is numerically stable when $P/Q \to 0$ as the X_i get large, as proves to be the case here.

This technique avoids the high degree of correlation between successive steps of a Markov chain walker; each sample is independently generated. This results in a much more rapid convergence for a given number of samples, and the stochastic behavior of the sampling process is familiar and obvious. It also requires far fewer evaluations of the posterior distribution function for the same number of samples, because the technique discards no samples, unlike MCMC. Benchmarking with posteriors that were exact MVNDs of dimension as large as 200 showed that this technique estimated the (exactly known) variances with uncertainties more than a factor of two better than achieved with MCMC for the same number of samples, in much less time.

There remains the question of choosing a suitable MVND for Q. In principle, any MVND that is not narrower than P will work, but for efficiency it should not be much broader, and should approximately duplicate the correlations in P. We have done this by generating a set of X_i for which P is not small, fitting a MVND to the set, and scaling up all the MVND widths by a small factor to suppress statistical fluctuations from the tail of Q.

To generate the set of X_i with significant value for P, we use MCMC, as we can use a smaller sample set, and we don't care as much about autocorrelation. We use 20 MCMC walkers to produce 5×10^4 R-matrix parameter sets, to which we fit an MVND using Mathematica [48]. We explored scaling factors from 0.5 to 1.5, and found that with scaling values less than 1, the statistical fluctuations in the sampling of the tail of Q were amplified by large values for W, producing large spikes in the W-weighted distributions. For scaling values greater than 1.1, the samples in the tail have very low weight, the fluctuations become very small, and the results are insensitive to the value of the scaling factor. For the high-quality MVND-based uncertainty quantification, we use a sample size of 2×10^5, a scaling factor of 1.2, and the statistical fluctuations are well controlled.

Typical results for this analysis are shown in Figs. 5 and 6, which demonstrate how close to Gaussian the resulting distributions are. The ANC(0^+), ANC(2^+), $S_{E2}(300)$, and $S_{E1}(300)$ values for each sample were weighted by W with a scaling factor of 1.2 and histogrammed to produce the sampled posterior distributions for these quantities. The error bars are the statistical uncertainties (the square root of the sum of the squared weights in each bin) and the weights are normalized so that the integral of each distribution is one. The red curves are χ^2-minimizing least squares fits of Gaussian functions to each distribution. The distributions for all other model parameters are of similar quality, with only mild skewness in a few cases. This justifies the use of the variance to define uncertainties, which we evaluate for all parameters and the astrophysical S factors through Eq. (14) and tabulate in Tables I, III, and V.

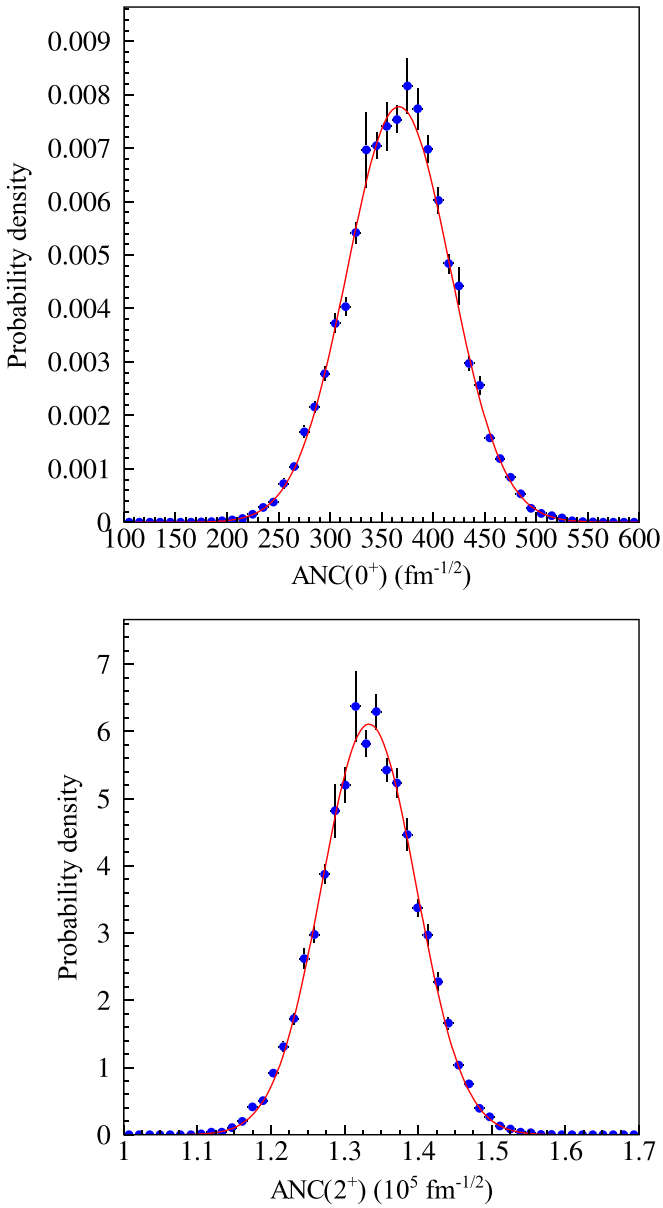

FIG. 5. ANC(0^+) (upper panel) and ANC(2^+) (lower panel) sampled posterior distributions with statistical uncertainties. The curves are Gaussians fit to the points.

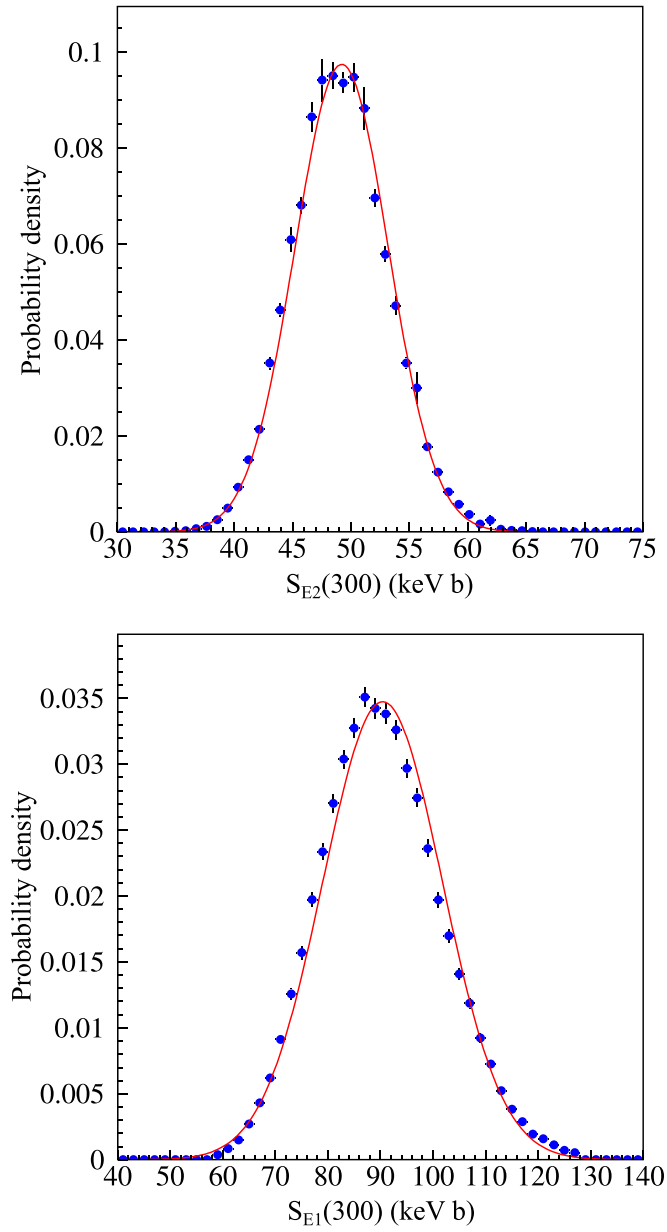

FIG. 6. SE2(300) (upper panel) and SE1(300) (lower panel) sampled posterior distributions with statistical uncertainties. The curves are Gaussians fit to the points. In the lower panel, the difference of 3 keV b between the mode of the posterior and the mean of the Gaussian is small compared to the 11 keV b standard deviation of the Gaussian.

Changes in some R-matrix parameters, for example ANC$p(0^+)$, produce only negligible changes in χ^2_{data}, so that the posterior is dominated by χ^2_{param}. We therefore expect the MAP fitting and the Bayesian uncertainty calculations to recover the literature values and uncertainties, which they do.

TABLE V. Fitted astrophysical S factors and uncertainties for the analysis of existing data. S is the sum of S_{E1} and S_{E2}, with uncertainties added in quadrature.

$S_{E1}(300)$	91 ± 12 keV b
$S_{E2}(300)$	48.9 ± 4.1 keV b
$S(300)$	140 ± 13 keV b

Other parameters that we excluded from χ^2_{param} (indicated by footnote 'a' in Tables I and III) are strongly constrained by the experimental data, resulting, in some cases, in uncertainties that are smaller than the literature results in [3]. Some of our uncertainties are strongly correlated, for example ANC(0^+) and ANC(2^+), as shown in Fig. 7. These correlations are entirely due to χ^2_{data}, as the terms in χ^2_{param} are explicitly uncorrelated.

We also note that the $S(300)$ distributions are also strongly correlated with some of the R-matrix parameters. S_{E2} is most

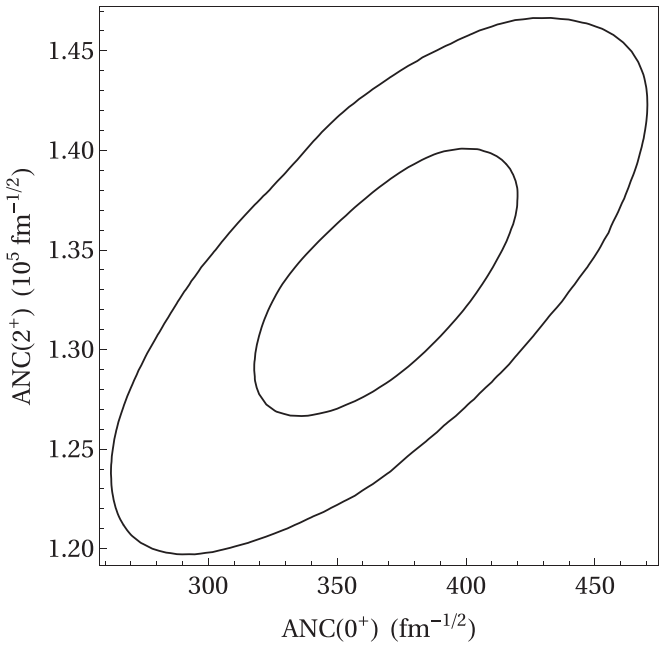

FIG. 7. 1σ (inner) and 2σ (outer) contours for the $E2$ posterior, projected into the ANC(0^+) (horizontal) vs ANC(2^+) (vertical) coordinates. The tilt indicates strong correlation between these parameters.

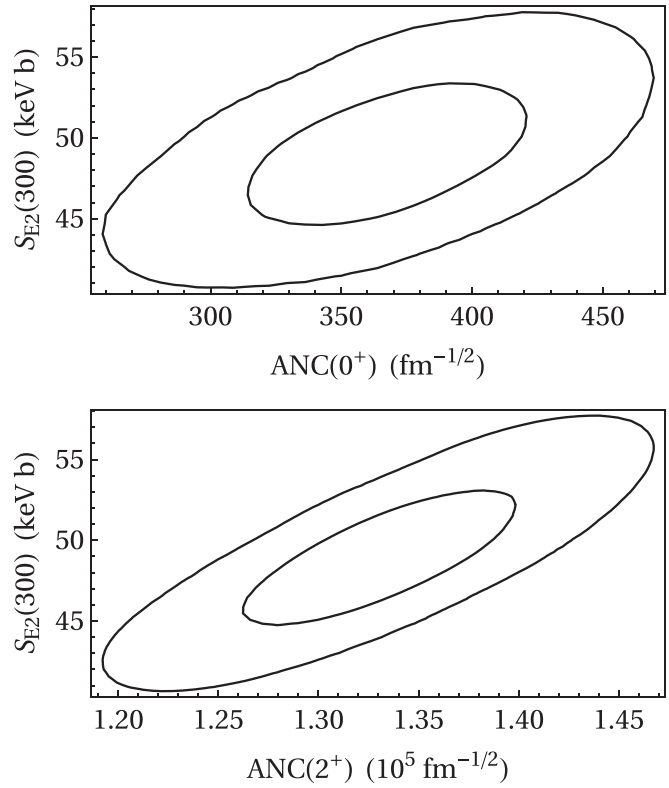

FIG. 8. 1σ (inner) and 2σ (outer) contours for the $E2$ posterior, projected into the $S_{E2}(300)$ versus ANC(0^+) coordinates (upper panel), and the $S_{E2}(300)$ versus ANC(2^+) coordinates (lower panel). The tilt indicates strong correlation.

strongly correlated with ANC(0^+) and ANC(2^+), as shown in Fig. 8. S_{E1} is most strongly correlated with ANC(1^-) and, interestingly, $\Gamma_{5\gamma}$, as shown in Fig. 9.

V. SIMULATED OSEEA DATA

All of the proceeding comprises a state-of-the-art baseline model for the existing CTAG data, to which we now add simulated OSEEA measurements. In [7,49], the authors develop a model for the OSEEA cross section that extrapolates the real-photon $E1$ and $E2$ multipoles to off-shell combinations of momentum and energy using a principle of "naturalness" to model the next-to-leading-order momentum transfer dependencies. They used these cross sections in a detailed Monte Carlo to calculate event yields corresponding to a proposed experiment, from which they inferred CTAG $E1$ and $E2S$ factors and statistical uncertainties. The proposed experiment featured a 114 MeV electron beam of 40 mA (corresponding to energy recovery linear accelerator CBETA [50]), passing through an oxygen jet target of thickness 5×10^{18} atoms/cm^2. Electrons were scattered at an angle of 15° with an integrated luminosity of 1.08×10^7 pb^{-1}, representing 100 days of running, with S factors determined over a center-of-mass energy range from 0.7 to 1.7 MeV in steps of 0.1 MeV.

For our Bayesian analysis, we require OSEEA data that lie exactly on the reference R-matrix model developed in the preceding sections, so that the new 'evidence' does not change the parameter values that maximize the posterior. It is also important that the OSEEA input model agrees with our reference R-matrix model for consistency in calculating the scattering cross sections from which the statistical uncertainties are derived. The previous work used a different R-matrix model than here; we have therefore repeated the OSEEA Monte Carlo simulation using $E1$ and $E2$ input data from the reference R-matrix model fitted above. In order to include planned capabilities of other energy recovery linear accelerators (e.g., MESA [51] and ARIEL [52]), the beam current for simulations in this paper was reduced to 10 mA (integrated luminosity over 100 d of 2.7×10^6 pb^{-1}) and detector acceptance was selected as defined in [53]. All other aspects of the simulation remain the same, apart from extending the energy range up to 6.35 MeV. We divide the results into two energy ranges: 'Low', for which $E_{\mathrm{low}} < 1.7$ MeV, and 'High', for which $E_{\mathrm{high}} > 1.7$ MeV. The low range corresponds to the energy range in [49].

To account for unmodeled additional sources of uncertainty, we added an additional constant statistical uncertainty in quadrature for each data point, and introduced a systematic normalization uncertainty in the Bayesian analysis, as we did for the existing data. We explored three values for these additional uncertainties: 2%, 5%, and 10%, for a total of nine combinations, representing optimistic to pessimistic outcomes in performing such an experiment. While these values are arbitrary, they serve as benchmarks to assess how easy or difficult it will be for an experiment like this to significantly improve our knowledge of the astrophysical S factors. The simulated OSEEA experiment results with 10% additional statistical uncertainty are plotted in Fig. 10.

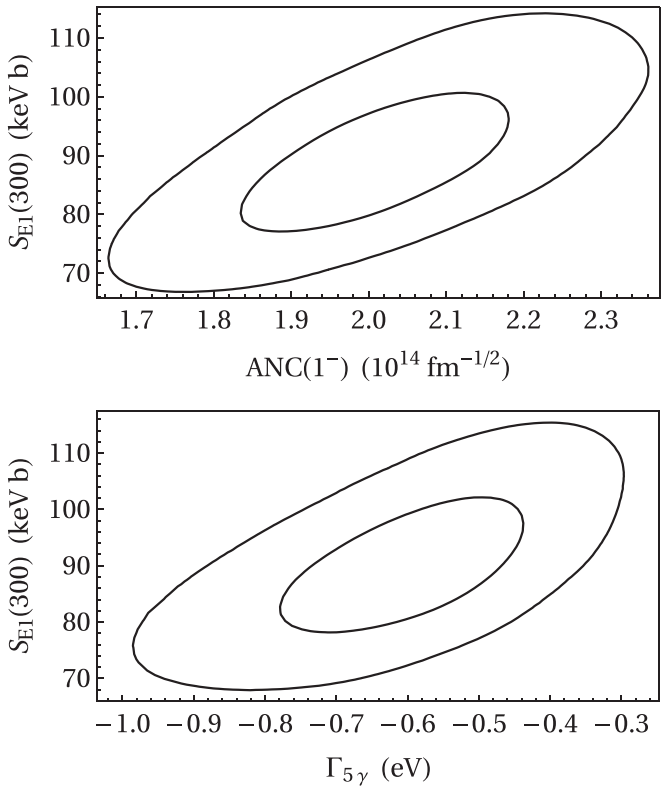

FIG. 9. 1σ (inner) and 2σ (outer) contours for the $E1$ posterior, projected into the $S_{E1}(300)$ versus ANC(1^-) coordinates (upper panel), and the $S_{E1}(300)$ versus $\Gamma_{5\gamma}$ coordinates (lower panel). The tilt indicates strong correlation.

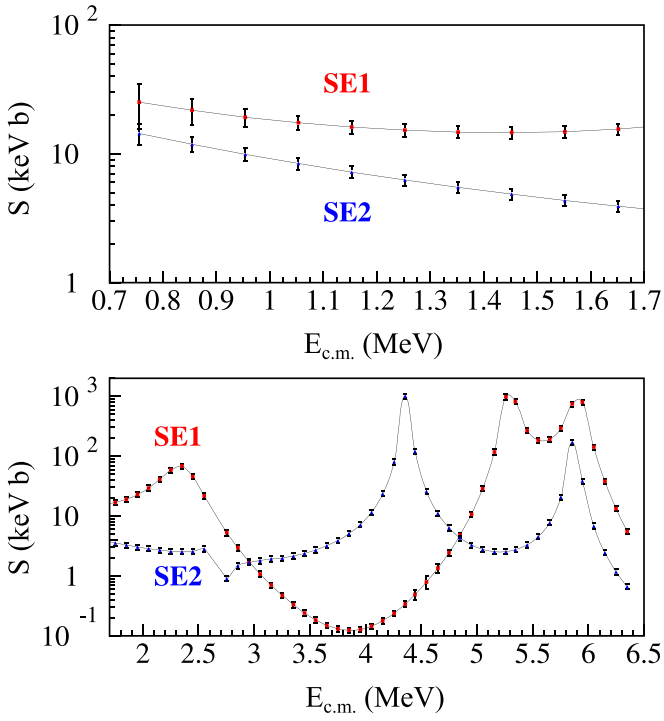

FIG. 10. Simulated OSEEA data combining statistical uncertainty with 10% additional uncertainty in quadrature. $E1$ data are plotted with red symbols; $E2$ with blue. The upper panel is for $E < 1.7$ MeV, and the lower for $E > 1.7$ MeV.

TABLE VI. $S_{E2}(300)$ uncertainties in keV b, calculated for existing data plus OSEEA data for different combinations of energy range (low, high, both), additional statistical uncertainty (2, 5, or 10 percent), and normalization uncertainty (2, 5, or 10 percent). These are to be compared with the results for existing data alone: $S_{E2}(300) = 48.9 \pm 4.1$ keV b.

OSEEA energy range	Normalization uncertainty		
and extra uncertainty	2%	5%	10%
Low, 2%	2.2	2.7	3.1
Low, 5%	2.5	2.9	3.5
Low, 10%	2.8	3.2	3.6
High, 2%	1.9	2.2	2.3
High, 5%	2.8	2.9	3.0
High, 10%	3.3	3.2	3.4
Both, 2%	1.4	1.8	2.0
Both, 5%	2.0	2.3	2.5
Both, 10%	2.6	2.8	2.9

VI. BAYESIAN UPDATING WITH SIMULATED OSEEA DATA

The new evidence from future OSEEA results is incorporated by adding an additional term into Eq. (8), which becomes

$$\chi^2_{\rm tot} = \chi^2_{\rm param} + \chi^2_{\rm data} + \chi^2_{\rm new}, \tag{15}$$

in which

$$\chi^2_{\rm new} = \sum \left(\frac{Y_i^{\rm new} - Y_i^{{\rm new},H}}{\Delta Y_i^{\rm new}} \right)^2, \tag{16}$$

where the $Y_i^{\rm new}$ are the simulated OSEEA data, $\Delta Y_i^{\rm new}$ are their uncertainties, and $Y_i^{{\rm new},H}$ are the values for a given hypothesis.

By construction, the MAP parameters are unchanged by introducing $\chi^2_{\rm new}$, because this term vanishes when the hypothesis is the previously fitted model. However, $\chi^2_{\rm new}$ will change the posterior for other hypotheses, and therefore will affect the uncertainties calculated for the model parameters and astrophysical S factors.

We have explored 27 different 'new' cases, formed by the three OSEEA energy ranges (low, high, and both together) and the nine different combinations of systematic and additional statistical uncertainties, to compare different experiment configurations and outcomes. For each test case, we use the same procedure of importance sampling with a MVND function that is fit to preliminary MCMC analysis of the posterior to calculate the variances of the model parameters and astrophysical S factors. As before, we used 2×10^5 samples with a scaling factor of 1.2 for the MVND widths. The resulting parameter distribution functions are again close to Gaussian in shape, although narrower in some cases than obtained for the existing data alone. The uncertainties calculated for the S factors are tabulated in Tables VI and VII; statistical uncertainties in these results are less than 0.1 keV b.

TABLE VII. $S_{E1}(300)$ uncertainties in keV b, calculated for existing data plus OSEEA data for different combinations of energy range (low, high, both), additional statistical uncertainty (2, 5, or 10 percent), and normalization uncertainty (2, 5, or 10 percent). These are to be compared with the results for existing data alone: $S_{E1}(300) = 91.4 \pm 11.7$ keV b.

OSEEA energy range	Normalization uncertainty		
and extra uncertainty	2%	5%	10%
Low, 2%	7.8	8.6	9.0
Low, 5%	8.3	9.3	9.9
Low, 10%	9.1	9.7	10.5
High, 2%	5.5	5.6	5.6
High, 5%	7.7	7.8	7.7
High, 10%	9.2	9.2	9.2
Both, 2%	3.6	3.9	4.0
Both, 5%	5.2	5.5	5.5
Both, 10%	6.9	7.1	7.2

VII. RESULTS AND SUMMARY

It is interesting to see how much the S factor uncertainties change when the OSEEA data are combined with the existing CTAG data. The additional data can only reduce the S factor uncertainties, but the improvement depends on the size of the statistical and systematic uncertainty in the new data. We can see that in general, as either the statistical or systematic uncertainty in the OSEEA data is decreased, the combined uncertainty in the S factors also decreases. However, there are some striking trends. In most cases, the combined S factor uncertainty using the high energy range data is as good or better than with the low energy range data; this holds for both $S_{E1}(300)$ and $S_{E2}(300)$. Also, for 10% normalization uncertainty in the OSEEA data (a typical value for most of the existing data), the improvement in S factor uncertainty for the low energy range is small in all cases.

These results demonstrate that to achieve significant improvement in S factor uncertainties from measurements in the low energy range alone will require extraordinary control of both statistical and systematic uncertainties. This, of course, is already well known from the long history of experimental work seeking to extend measurements to ever lower energies. However, these results also show that significant progress can be made with measurements in the high energy range with much less stringent requirements on the experimental uncertainties. Moreover, experiments at higher energies are easier to perform because of the larger cross sections. This suggests that new experiments should not overlook making measurements at higher energies. For example, we find that the proposed OSEEA experiment over the full energy range could cut the uncertainty in half when combined with the existing data, assuming 10% systematic uncertainty and an additional 2% increase in statistical uncertainty. These results may give guidance in designing new experiments to study the CTAG reaction at stellar energies, and we look forward to new data that will improve our understanding of this important astrophysical reaction.

ACKNOWLEDGMENTS

We thank R. J. deBoer and K. Fossez for useful discussions. This work is supported by the U.S. National Science Foundation under Grants No. 1812340 and No. 2110898, the U.S. Department of Energy (DOE), Office of Science, Office of Nuclear Physics, under Contract No. DE-AC02-06CH11357, and the Croatian Science Foundation under the Project No. IP-2022-10-3878.

[1] W. A. Fowler, Experimental and theoretical nuclear astrophysics: The quest for the origin of the elements, Rev. Mod. Phys. **56**, 149 (1984).

[2] S. E. Woosley, A. Heger, T. Rauscher, and R. D. Hoffman, Nuclear data needs for the study of nucleosynthesis in massive stars, Nucl. Phys. A **718**, 3 (2003).

[3] R. J. deBoer, J. Görres, M. Wiescher, R. E. Azuma, A. Best, C. R. Brune, C. E. Fields, S. Jones, M. Pignatari, D. Sayre, K. Smith, F. X. Timmes, and E. Uberseder, The $^{12}C(\alpha,\gamma)^{16}O$ reaction and its implications for stellar helium burning, Rev. Mod. Phys. **89**, 035007 (2017).

[4] B. T. Pepper, A. G. Istrate, A. D. Romero, and S. O. Kepler, The impact of the uncertainties in the 12C(α, γ)16O reaction rate on the evolution of low- to intermediate-mass stars, Mon. Not. R. Astron. Soc. **513**, 1499 (2022).

[5] R. Farmer, M. Renzo, S. de Mink, M. Fishbach, and S. Justham, Constraints from gravitational wave detections of binary black hole mergers on the $^{12}C(\alpha,\gamma)^{16}O$ rate, Astrophys. J. Lett. **902**, L36 (2020).

[6] K. Belczynski, The most ordinary formation of the most unusual double black hole merger, Astrophys. J. Lett. **905**, L15 (2020).

[7] I. Friščić, T. W. Donnelly, and R. G. Milner, New approach to determining radiative capture reaction rates at astrophysical energies, Phys. Rev. C **100**, 025804 (2019).

[8] C. Ugalde, B. DiGiovine, R. J. Holt, D. Henderson, K. E. Rehm, R. Suleiman, A. Freyberger, J. Grames, R. Kazimi, M. Poelker, R. Mammei, D. Meekins, Y. Roblin, A. Sonnenschein, and A. Robinson, Measurement of $^{16}O(\gamma,\alpha)^{12}C$ with a bubble chamber and a bremsstrahlung beam (2013), Jefferson Lab Proposal No. PR12-13-005, https://www.jlab.org/exp_prog/proposals/13/PR12-13-005.pdf.

[9] Y. Xu, W. Xu, Y. G. Ma, W. Guo, Y. G. Chen, X. Z. Cai, H. W. Wang, C. B. Wang, G. C. Lu, and W. Q. Shen, A new study for $^{16}O(\gamma,\alpha)^{12}C$ at the energies of nuclear astrophysics interest: The inverse of key nucleosynthesis reaction $^{12}C(\alpha,\gamma)^{16}O$, Nucl. Instrum. Methods Phys. Res. A **581**, 866 (2007).

[10] M. Gai, Nuclear astrophysics with Gamma-beams, J. Phys.: Conf. Ser. **1078**, 012011 (2018).

[11] D. L. Balabanski, R. Popescu, D. Stutman, K. A. Tanaka, O. Tesileanu, C. A. Ur, D. Ursescu, and N. V. Zamfir, New light in nuclear physics: The extreme light infrastructure, Europhys. Lett. **117**, 28001 (2017).

[12] D. Neto, K. Bailey, J. F. Benesch, B. Cade, B. DiGiovine, A. Freyberger, J. M. Grames, A. Hofler, R. J. Holt, R. Kazimi, D.

Meekins, M. McCaughan *et al.*, Measuring the cross section of the $^{15}N(\alpha,\gamma)^{19}F$ reaction using a single-fluid bubble chamber, Phys. Rev. C **107**, 035801 (2023).
[13] D. Budker, J. R. C. López-Urrutia, A. Derevianko, V. V. Flambaum, M. W. Krasny, A. Petrenko, S. Pustelny, A. Surzhykov, V. A. Yerokhin, and M. Zolotorev, Atomic physics studies at the Gamma Factory at CERN, Ann. Phys. **532**, 2000204 (2020).
[14] O. Adriani *et al.*, Technical Design Report EuroGammaS proposal for the ELI-NP Gamma beam System, arXiv:1407.3669.
[15] P. S. Tracz, ELI-NP Gamma beam system - Current project status, in *Proc. LINAC'18*, Linear Accelerator Conference, Vol. 29 (JACoW Publishing, Geneva, Switzerland, 2019), paper MOPO009, pp. 59–61.
[16] R. E. Azuma, E. Uberseder, E. C. Simpson, C. R. Brune, H. Costantini, R. J. de Boer, J. Görres, M. Heil, P. J. LeBlanc, C. Ugalde, and M. Wiescher, AZURE: An R-matrix code for nuclear astrophysics, Phys. Rev. C **81**, 045805 (2010).
[17] R. J. Holt, B. W. Filippone, and S. C. Pieper, Impact of $^{16}O(\gamma,\alpha)^{12}C$ measurements on the $^{12}C(\alpha,\gamma)^{16}O$ astrophysical reaction rate, Phys. Rev. C **99**, 055802 (2019).
[18] R. J. Holt, B. W. Filippone, and S. C. Pieper, Sensitivity study for the $^{12}C(\alpha,\gamma)^{16}O$ astrophysical reaction rate, arXiv:1809.10176.
[19] R. J. Holt and B. W. Filippone, Impact of $^{16}O(e,e'\alpha)^{12}C$ measurements on the $^{12}C(\alpha,\gamma)^{16}O$ astrophysical reaction rate, Phys. Rev. C **100**, 065802 (2019).
[20] R. J. Holt, H. E. Jackson, Jr., R. M. Laszewski, J. E. Monahan, and J. R. Specht, Effects of channel and potential radiative transitions in the $^{17}O(\gamma,n_0)^{16}O$ reaction, Phys. Rev. C **18**, 1962 (1978).
[21] D. R. Tilley, H. R. Weller, and C. M. Cheves, Energy levels of light nuclei A = 16-17, Nucl. Phys. A **564**, 1 (1993).
[22] R. T. Birge, The calculation of errors by the method of least squares, Phys. Rev. **40**, 207 (1932).
[23] C. R. Brune, W. H. Geist, R. W. Kavanagh, and K. D. Veal, Sub-Coulomb alpha transfers on ^{12}C and the $^{12}C(\alpha,\gamma)^{16}O$ S factor, Phys. Rev. Lett. **83**, 4025 (1999).
[24] L. Buchmann, R. Azuma, C. Barnes, J. Humblet, and K. Langanke, Present experimental constraints on the total S-factor of $^{12}C(\alpha,\gamma)^{16}O$ and proposals for future experiments, Nucl. Phys. A **621**, 153 (1997).
[25] Y. P. Shen *et al.*, Astrophysical S_{E2} factor of the $^{12}C(\alpha,\gamma)^{16}O$ reaction through the $^{12}C(^{11}B,^{7}Li)^{16}O$ transfer reaction, Phys. Rev. C **99**, 025805 (2019).
[26] A. Belhout, S. Ouichaoui, H. Beaumevieille, A. Boughrara, S. Fortier, J. Kiener, J. Maison, S. Mehdi, L. Rosier, J. Thibaud, A. Trabelsi, and J. Vernotte, Measurement and DWBA analysis of the $^{12}C(^{6}Li,\ d)^{16}O$ α -transfer reaction cross sections at 48.2 MeV: R-matrix analysis of $^{12}C(\alpha,\gamma)^{16}O$ direct capture reaction data, Nucl. Phys. A **793**, 178 (2007).
[27] C. Matei, C. R. Brune, and T. N. Massey, Present experimental constraints on the total S-factor of $^{12}C(\alpha,\gamma)^{16}O$ and proposals for future experiments, Phys. Rev. C **78**, 065801 (2008).
[28] P. Tischhauser, A. Couture, R. Detwiler, J. Görres, C. Ugalde, E. Stech, M. Wiescher, M. Heil, F. Käppeler, R. E. Azuma, and L. Buchmann, Measurement of elastic $^{12}C+\alpha$ scattering: Details of the experiment, analysis, and discussion of phase shifts, Phys. Rev. C **79**, 055803 (2009).
[29] N. Oulebsir, F. Hammache, P. Roussel, M. G. Pellegriti, L. Audouin, D. Beaumel, A. Bouda, P. Descouvemont, S. Fortier, L. Gaudefroy, J. Kiener, A. Lefebvre-Schuhl, and V. Tatischeff, Indirect study of the $^{12}C(\alpha,\gamma)^{16}O$ reaction via the $^{12}C(^{7}Li,t)^{16}O$ transfer reaction, Phys. Rev. C **85**, 035804 (2012).
[30] M. L. Avila, G. V. Rogachev, E. Koshchiy, L. T. Baby, J. Belarge, K. W. Kemper, A. N. Kuchera, A. M. Mukhamedzhanov, D. Santiago-Gonzalez, and E. Uberseder, Constraining the 6.05 MeV 0^+ and 6.13 MeV 3^- cascade transitions in the $^{12}C(\alpha,\gamma)^{16}O$ reaction using the asymptotic normalization coefficients, Phys. Rev. Lett. **114**, 071101 (2015).
[31] S. Adhikari, C. Basu, P. Sugathan, A. Jhinghan, B. R. Behera, N. Saneesh, G. Kaur, M. Thakur, R. Mahajan, R. Dubey, and A. K. Mitra, Breakup effects on alpha spectroscopic factors of 16O, J. Phys. G: Nucl. Part. Phys. **44**, 015102 (2017).
[32] Y. P. Shen, B. Guo, R. J. deBoer, Z. H. Li, Y. J. Li, X. D. Tang, D. Y. Pang, S. Adhikari, C. Basu, J. Su, S. Q. Yan, Q. W. Fan, J. C. Liu, C. Chen, Z. Y. Han, X. Y. Li, G. Lian, T. L. Ma, W. Nan, W. K. Nan *et al.*, Constraining the external capture to the ^{16}O ground state and the $E2S$ factor of the $^{12}C(\alpha,\gamma)^{16}O$ reaction, Phys. Rev. Lett. **124**, 162701 (2020).
[33] A. K. Mondal, C. Basu, S. Adhikari, C. Bhattacharya, T. K. Rana, S. Kundu, S. Manna, R. Pandey, P. Roy, A. Sen, J. K. Meena, A. K. Saha, J. K. Sahoo, D. Basak, T. Bar, H. Pai, A. Bisoi, A. K. Mitra, and P. Biswas, $^{12}C(^{20}Ne,^{16}O)^{16}O$ α-transfer reaction and astrophysical S-factors at 300keV, Int. J. Mod. Phys. E **30**, 2150039 (2021).
[34] J. M. L. Ouellet, H. C. Evans, H. W. Lee, J. R. Leslie, J. D. MacArthur, W. McLatchie, H.-B. Mak, P. Skensved, J. L. Whitton, X. Zhao, and T. K. Alexander, $^{12}C(\alpha,\gamma)^{16}O$ cross sections at stellar energies, Phys. Rev. Lett. **69**, 1896 (1992).
[35] G. Roters, C. Rolfs, F. Strieder, and H. Trautvetter, measurement of the $^{16}O(e,e'\alpha)^{12}C$, Eur. Phys. J. A **6**, 451 (1999).
[36] R. Kunz, M. Jaeger, A. Mayer, J. W. Hammer, G. Staudt, S. Harissopulos, and T. Paradellis, $^{12}C(\alpha,\gamma)^{16}O$: The key reaction in stellar nucleosynthesis, Phys. Rev. Lett. **86**, 3244 (2001).
[37] M. Assunção *et al.*, E1 and E2 S factors of $^{12}C(\alpha,\gamma_0)^{16}O$ from γ-ray angular distributions with a 4 π-detector array, Phys. Rev. C **73**, 055801 (2006).
[38] H. Makii, Y. Nagai, T. Shima, M. Segawa, K. Mishima, H. Ueda, M. Igashira, and T. Ohsaki, E-1 and E-2 cross sections of the $^{12}C(\alpha,\gamma_0)^{16}O$ reaction using pulsed alpha beams, Phys. Rev. C **80**, 065802 (2009).
[39] D. Schürmann, A. Di Leva, L. Gialanella, R. Kunz, F. Strieder, N. De Cesare, M. De Cesare, A. D'Onofrio, K. Fortak, G. Imbriani, D. Rogalla, M. Romano, and F. Terrasi, Study of the 6.05 MeV cascade transition in $^{12}C(\alpha,\gamma)^{16}O$, Phys. Lett. B **703**, 557 (2011).
[40] R. Plag, R. Reifarth, M. Heil, F. Kappeler, G. Rupp, F. Voss, and K. Wisshak, $^{12}C(\alpha,\gamma)^{16}O$ studied with the Karlsruhe 4π BaF_2 detector, Phys. Rev. C **86**, 015805 (2012).
[41] F. Brochard, P. Chevallier, D. Disdier, V. Rauch, and F. Scheibling, Étude des désexcitations électromagnétiques des niveaux 1- situés à 12,44 et 13,09 MeV dans le noyau 16O, J. Phys. France **34**, 363 (1973).
[42] P. Dyer and C. A. Barnes, The $^{12}C(\alpha,\gamma)^{16}O$ reaction and stellar helium burning, Nucl. Phys. A **233**, 495 (1974).
[43] R. M. Kremer, C. A. Barnes, K. H. Chang, H. C. Evans, B. W. Filippone, K. H. Hahn, and L. W. Mitchell, Coincidence measurement of the $^{12}C(\alpha,\gamma)^{16}O$ cross section at low energies, Phys. Rev. Lett. **60**, 1475 (1988).

[44] A. Redder, H. W. Becker, C. Rolfs, H. P. Trautvetter, T. R. Donoghue, T. C. Rinckel, J. W. Hammer, and K. Langanke, The $^{12}C(\alpha,\gamma)^{16}O$ cross section at stellar energies, Nucl. Phys. A **462**, 385 (1987).

[45] L. Gialanella *et al.*, A new measurement of the E1 amplitude in $^{12}C(\alpha,\gamma_0)^{16}O$, Nucl. Phys. A **688**, 254 (2001).

[46] D. Sivia and J. Skilling, *Data Analysis: A Bayesian Tutorial*, 2nd ed. (Oxford University Press, Oxford, 2006).

[47] D. Abramson, T. Peachey, and A. Lewis, Model Optimization and parameter estimation with Nimrod/O, in *Computational Science — ICCS 2006*, edited by V. N. Alexandrov, G. D. van Albada, P. M. A. Sloot, and J. Dongarra (Springer, Berlin, Heidelberg, 2006), pp. 720–727.

[48] Wolfram Research, Inc., Mathematica, version 14.1, Champaign, IL (2024).

[49] I. Friščić, T. W. Donnelly, and R. G. Milner, A new approach to determine the $^{12}C(\alpha,\gamma)^{16}O$ reaction rate at astrophysical energies, J. Phys.: Conf. Ser. **1643**, 012056 (2020).

[50] A. Bartnik *et al.*, CBETA: First multipass superconducting linear accelerator with energy recovery, Phys. Rev. Lett. **125**, 044803 (2020).

[51] F. Hug, K. Aulenbacher, R. G. Heine, B. Ledroit, and D. Simon, MESA - an ERL project for particle physics experiments, in *Proceedings of the Linear Accelerator Conference (LINAC'16)*, Linear Accelerator Conference, Vol. 28 (JACoW, Geneva, Switzerland, 2017), paper MOP106012, pp. 313–315.

[52] R. Laxdal, Z. Ang, T. Au, K. Fong, O. Kester, S. Koscielniak, A. Koveshnikov, M. Laverty, Y. Ma, D. Storey, E. Thoeng, Z. Yao, Q. Zheng, and V. Zvyagintsev, The 30 MeV stage of the ARIEL e-linac, in *Proceedings of the 18th International Conference on RF Superconductivity (SRF'17), Lanzhou, China, July 17–21, 2017*, International Conference on RF Superconductivity No. 18, edited by R. W. S. Volker, Y. He, L. Li, and N. Zhao (JACoW, Geneva, Switzerland, 2018), pp. 6–12.

[53] I. Friščić, T. Donnelly, and R. Milner, Electrodisintegration of ^{16}O and determination of astrophysical S-factors of the inverse reaction, J. Phys.: Conf. Ser. **2391**, 012018 (2022).